**International Journal of Electrical and Computer Engineering (IJECE)**
Vol. 5, No. 6, December 2015, pp. 1262~1274
ISSN: 2088-8708


# Numerical and Experimental Investigation of Bridge Currents of an Induction Machine Equipped with Bridge Configured Winding

**Sivaramakrishnan Natesan*, Karuna Kalita*, Venkatesu Samala****
* Department of Mechanical Engineering, Indian Institute of Technology Guwahati, India
** ICON Design and Automation,Bangalore, India

**Article Info**

***Article history:***

Received May 25, 2015
Revised Jul 14, 2015
Accepted Aug 3, 2015

***Keyword:***

Bridge Configured Winding
Finite Element Simulation
Induction machine
Unbalanced Magnetic Pull

**ABSTRACT**

An eccentric rotor motion imbalances the magnetic field distribution in the air-gap region. Due to this uneven flux density distribution, a net radial force called Unbalanced Magnetic Pull (UMP) is in action towards the shortest air-gap. This UMP can degrade the machine's performance. UMP can be controlled by a special kind of winding called Bridge Configured Winding (BCW). The BCW winding is a single set of winding which is used to produce the torque as well as the controllable force. The main contribution of this paper is to inspect the flow of bridge currents in the bridges when the machine is having rotor eccentricity or unbalance. The bridge currents in the presence of rotor eccentricity with the stator of an Induction machine model has been analyzed by using an Electromagnetic Finite Element (FE) solver called Opera 2D/RM solver (Rotation Motion Analysis). The bridge currents have been measured for two different cases, (i) Induction machine model with zero eccentricity, (ii) Induction machine model with 10% static eccentricity of the air gap. Experimental results are presented for the validation of Opera 2D/RM results. A modified 37kW Induction machine has been used for this study. A known mass unbalance is introduced in the perforated disc in order to create the unbalance in the system purposefully. The bridge currents have been measured and compared with and without unbalance present in the system. The comparison of measured bridge currents for all the cases are given in the frequency domain.



***Corresponding Author:***

Karuna Kalita,
Department of Mechanical Engineering, Indian Institute of Technology, Guwahati,
Assam-781039, India, +91-361-2582680.
Email: karuna.kalita@iitg.ernet.in

## 1. INTRODUCTION

In electrical machines UMP occurs due to the rotor eccentricity present in the system and it tends to further increase the rotor eccentricity. This may lead to the excessive vibration, stator and rotor rubbing, and wear of bearing. It may reduce the machine's performance, if they are not sufficiently controlled. So, it is very important to know about the dynamic behavior of UMP acting on the rotor during the design process and construction of a high speed rotating machines. Over hundred years ago, many researchers have studied about the source and the nature of the UMP and how it can be minimized. The UMP can be controlled by some special kind of winding schemes such as dual set of stator winding, single set of stator winding, damper winding, series and parallel winding, equalizing connections in parallel winding which are presented in [1]. BCW is a single set of winding which can be used as a built-in force actuator. The important feature of this type of winding connection is that it requires a relatively low current and low voltage for the lateral force production. It can eliminate the drawbacks by using dual set of winding connection. The lateral force

production has been explained in [2], [3] by the BCW in a poly phase induction machine for active vibration control. The dynamics of the bridge configured built-in force is presented in [4]. An analytical model has been used to control the flexural vibration in BCW based cage induction machine by this lateral force. The present paper describes the modeling and simulation of a bridge configured winding based induction machine by using Opera 2D/RM solver.

The real time engineering problems have been successfully applied in numerical methods with the help of modern high speed digital computers. Finite Element Method is one of the important numerical methods which provide computational techniques for the analysis and the solution of the mathematical problems. During recent decades, the use of FEM tool for the numerical simulation has become more popular because of its wide range of applications. The utilization of commercial software is now available for the implementation of Finite Element techniques. Opera FEM software is one of the finest tools for the 2D and 3D electromagnetic analysis. Most of the finite element problems have been solved by 2D solver in order to avoid the complexity in nature as well as the time and the cost. Comparatively few literatures have been studied about the new winding scheme called BCW as well as the utilization of Opera 2D and 3D FE Software for an electromagnetic analysis. An effect of discretization of the 2D induction machine model and the simulation of 3D Opera FE Model has been presented in [5], [6]. It uses the multi-slice model with the straight rotor bar for the discretization of 2D model which can provides the 3D environment. The results of 2D model have been compared with the results of 3D skewed rotor bar model. The result shows that the skewed rotor bar reduces the rotor bar currents. The verification of field-circuit FM models of an induction motor is described in [7] by using Opera 2D steady state (AC) solver and Transient analysis (RM analysis) methods with the experimental results. The machine performance was also studied by DC impulse test. The characterization of machine behavior has been presented in [8]-[10]. The machine parameters such as efficiency, torque, power loss and winding currents have been measured and compared at various slip for different rotor bar materials and different rotor steel sheet thickness. Analysis has been done for 0.35mm and 0.50mm non oriented steel sheet thickness of rotor core laminations are showed in [9]. It can be noticed that the results of 0.35mm thickness rotor core lamination model has good agreements than 0.50mm thickness rotor core lamination model. Simulation has been done for aluminium and copper rotor bar material induction machine models are presented in [10]. The results show the copper rotor bar is better than aluminium rotor bar. Modeling and simulation of a synchronous generator, Induction machine and a reciprocating actuator by Opera 2D for the machine characterization have been presented in [11]. Opera 2D/RM analysis has been included for the effect of rotor, rotor skewness, and rotor slotting. The utilization of in built rotor bar models in the library of Opera 2D software has been used in [12] for the Induction machine analysis. Torque, stator current and ohmic losses have been calculated for all the models and compared with each other. A time stepping finite element method has been used in [13] for the electromagnetic analysis of a bridge configured based Induction machine. It can be observed that the frequency component of UMP due to eccentricity has good agreements with the analytical and experimental results. An experimental setup has been demonstrated in [1] for the unbalance detection in a bridge configured induction machines. The equalizing currents or bridge currents flows in the system due to unbalance present in the system. The equalizing current or bridge current can be used as a measure of unbalance present in the system.

The characterization of an induction machine and the machine's performance has been analyzed by using different conductor material, different rotor core lamination material, different cross section of rotor bars and multislice method in Opera FE software are considered in the existing work. However, there is no implementation of the bridge configured winding scheme along with the double layered stator winding. The main contribution of the present work is that to analyze the effect of rotor eccentricity or unbalance in the system on the bridge currents in a BCW based Induction motor. The numerical results from Opera 2D/RM have been validated with the experimental results. This paper has been divided into six sections. The literature review to the current work has been presented in Section 1. Section 2 explains the working principle of Bridge Configured Winding scheme. Section 3 illustrates the modeling and analysis of an Induction machine in Opera 2D which elaborates the transient analysis (RM Analysis). Also, the modeling of an air gap region and winding connection in Opera 2D external circuit editor has been presented in this section. The induction machine has been modeled for two different cases such as, (i) Zero eccentricity model, (ii) 10% static eccentricity model. The 10% rotor eccentricity is given in the negative Y- direction. Section 4. demonstrates the experimental rig set up. The comparison of obtained Opera 2D/RM results, validation of Opera 2D results with the experimental results and conclusion are presented in Section 5. and Section 5.5. respectively.

## 2. BRIDGE CONFIGURED WINDING

The BCW can be used as a built-in force actuator. BCW can produce both torque as well as a controllable transverse force. Figure 1 shows the double layered distributed three phase, four pole winding. The stator winding connection has been done according to the circuit connection as shown in Figure 2. An additional 2-pole field has been introduced purposefully with the 4-pole fundamental field by short circuiting the bridges. By, superimposition of this 2-pole field and 4-pole field can produce a force called levitation force which can be used to counteract the UMP which is already present in the system. BCW can provide both the three phase motor supply $(i_{Aph}, i_{Bph}, \text{and } i_{Cph})$ and three isolated levitation power supply $(i_{Alev}, i_{Blev}, \text{and } i_{Clev})$. The fact that it can be possible to generate the radial forces by shot-circuiting the bridges S1, S2 and S3.

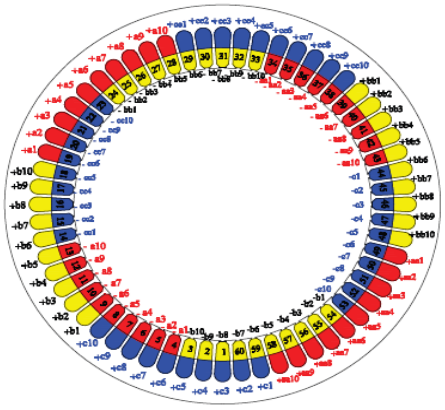

Figure 1. A winding scheme of a distributed double layered winding

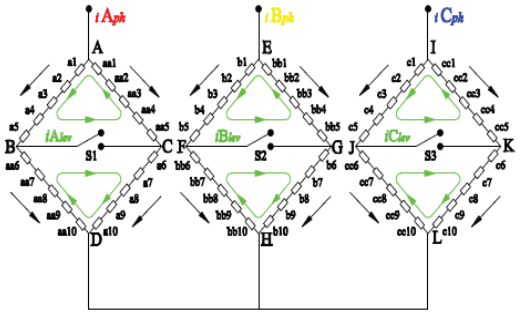


Figure 2. A bridge configured winding circuit

The current responsible for the torque production are divided into two parallel paths in each phase. Consider the Phase-A winding connection of the induction motor, with two parallel branches comprising ten series-connected coils each, shown in Figure 2. The currents flowing in the arm AB and CD are same in direction and magnitude but both the arms were connected in diametrically opposite to each other at a span of $180^{o}$. Similarly, AC and BD arms were connected in the same fashion. The branches AB and CD have the same polarity while both branches AC and BD have the opposite polarity with respect to AB and CD. The branches AB and CD have similar feature and they can be grouped together. Likewise, branches AC and BD are set to be an another group. These two coil groups are placed diametrically opposite to each other in the stator slots. The current flowing across BC is called levitation current or bridge current and it is very small when compared to the current flowing across AD i.e., called main supply current.

### 2.1. Working Principle of Bridge Configured Winding

An uneven flux density distribution due to rotor eccentricity or unbalance present in the system can produce an additional flux of pole pair $(p\pm1)$ (where, p is the number of fundamental pole pairs). Any one of this additional flux pole pair can interact with the fundamental pole pair flux, a significant net transverse force (UMP) can be produced. BCW scheme works on this principle. An additional 2-pole field has been introduced purposefully with the 4-pole fundamental field by short circuiting the bridges. By superimposing this 2-pole field and 4-pole field, a levitation force can be produced to counteract the UMP which is already present in the system. The induced bridge currents have the capability of producing an additional 2-pole and 6-pole magnetic flux density components. These 2-pole and 6-pole fields can interact with the 4-pole main field and thus a radial magnetic flux density can be produced in the air gap. The radial magnetic flux density by the 2-pole, 4-pole and 6-pole fields has been given by equation (1) which is presented in [4].

$$B(t,\varphi) = \mathrm{Re}\left\{\underline{\hat{B}}_1(t)\, e^{-j\varphi} + \underline{\hat{B}}_2(t)\, e^{-j2\varphi} + \underline{\hat{B}}_3(t)\, e^{-j3\varphi}\right\} \quad (1)$$

Where, $t$ is the time, $\varphi$ denotes the angular co-ordinate along the rotor periphery, $\underline{\hat{B}}_1$, $\underline{\hat{B}}_2$ and $\underline{\hat{B}}_3$ are the space vectors of the 2-pole, 4-pole and 6-pole magnetic flux density distribution in the air gap respectively.

Consider the Phase A winding connection of the Induction machine shown in Figure 1. When the Induction machine is supplied with the main supply, the current will flow through the arm AB and BD in one path as well as AC and CD in an another path. A four pole field has been formed according to the winding pattern as shown in Figure 3. It has been realized that the presence of unbalance in the system, the current will flow through the arm BC [2] as soon as it is being short circuited and it is called as levitation current $i_{Alev}$. The levitation current $i_{Alev}$ will flow in the arm AB through the arm CA in order to make a closed loop path. Similarly, the levitation current $i_{Alev}$ will flow in the arm DB through CD. It has been observed in the arms AC and BD that the levitation current $i_{Alev}$ flows in the opposite direction to the direction of main supply current $i_{Aph}$ shown in Figure 2. The polarity of the current flowing in the arms AC and BD have been reversed due the opposite direction of flow of levitation current which is shown in Figure 4, and thus the 2-pole field has been formed. The super imposed levitation field is a pole pair different with the main pole pair field. As a result, a net transverse force called levitation force is exerted on the rotor as shown in Figure 5. Therefore, a levitation force can be produced in any arbitrary direction with the combination of bridge connections. The levitation force production by the interaction of a difference of one pole pair between the fields has been proved mathematically in [2].

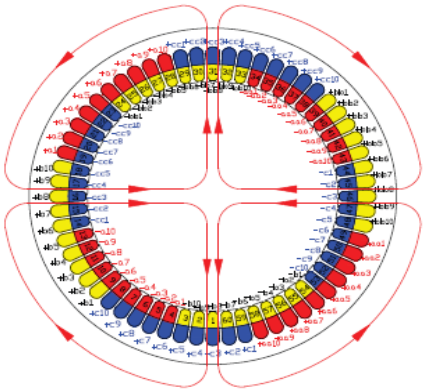

Figure 3. Main 4-Pole field formation

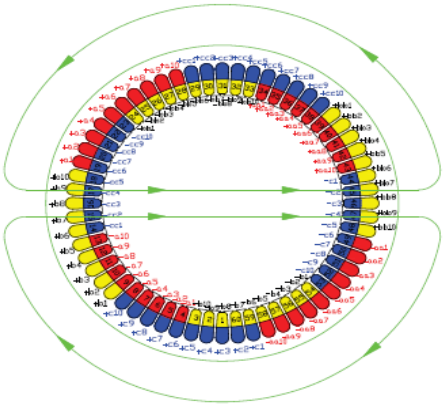

Figure 4. 2-Pole field formation

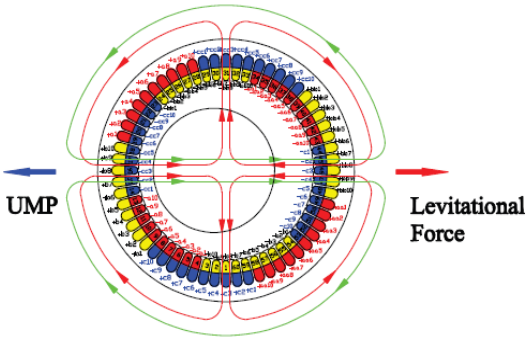


Figure 5. Superimposition of 4-Pole and 2-Pole fields

## 3. OPERA 2D FINITE ELEMENT MODELING

### 3.1. Transient Analysis of the Induction Machine

Rotating motion analysis (RM) is used for the transient analysis of the induction machine. Figure 6 shows the induction machine model with BCW scheme. The machine parameters are given in Table 1. The cross sections of stator slot and rotor bar are given in Figure 7 and Figure 8 respectively. The induction machine model has 60 stator slots and 48 rotor slots. A non linear material property has been given to the stator and rotor core.

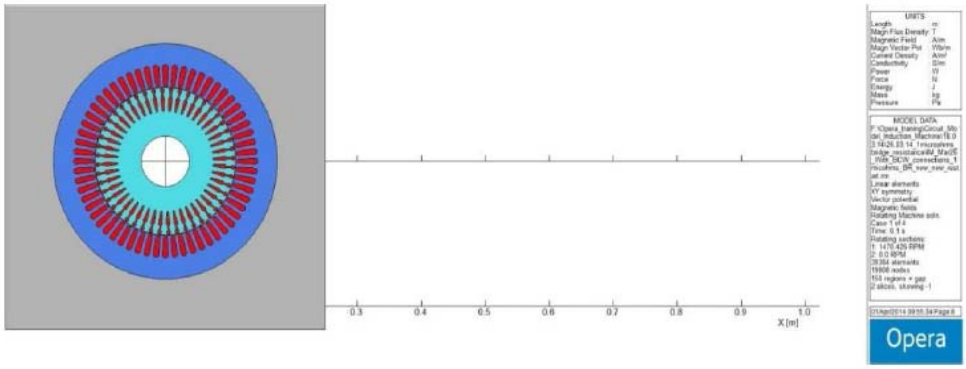


Figure 6. Opera 2D Induction machine model with BCW

Table 1. Machine Parameters

| Sl No | Parameter | Value |
|---|---|---|
| 1 | Stator outer diameter | 350.0 mm |
| 2 | Stator inner diameter | 221.0 mm |
| 3 | Stator core length | 212.0 mm |
| 4 | Rotor outer diameter | 218.5 mm |
| 5 | Rotor inner diameter | 75.0 mm |
| 6 | Rotor skew | 5o |
| 7 | Airgap | 1.25 mm |

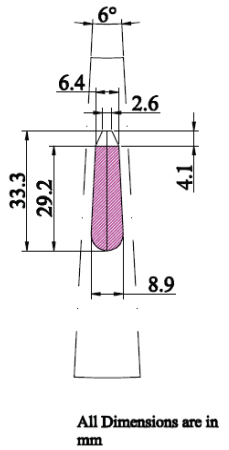


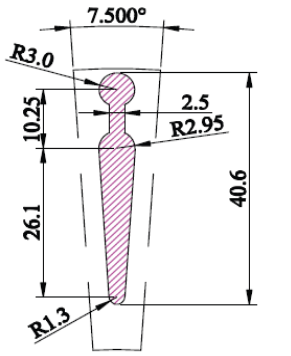


Figure 7. A stator slot dimension Figure 8. A rotor bar dimension

The rotating parts are rotating relatively with the stationary parts. The important feature of this FEM tool is that it can rearrange the mesh in the air-gap region in order to rejoin the rotating elements with the stationary elements after every rotation with an adjoining mesh. The FEM model has one air-gap region to separate the stator and rotor parts in order to form the stator air gap region and rotor air gap region as shown in Figure 9. The air-gap of the induction machine is ”1.25mm”. The air-gap is divided into three equal regions in order to create the annular air-gap region of ”0.426667mm” for stator air-gap and rotor air-gap region. It is important to give midair-gap radius so that Opera 2D/RM can create the air polygon in between stator air-gap region and rotor air-gap region. The midair-gap radius of the model is ”109.875mm”. Triangular element has been chosen for the mesh. The complete model comprises of 19808 nodes and 39384 elements. Figure 10 shows the close view of the mesh in the air-gap region.

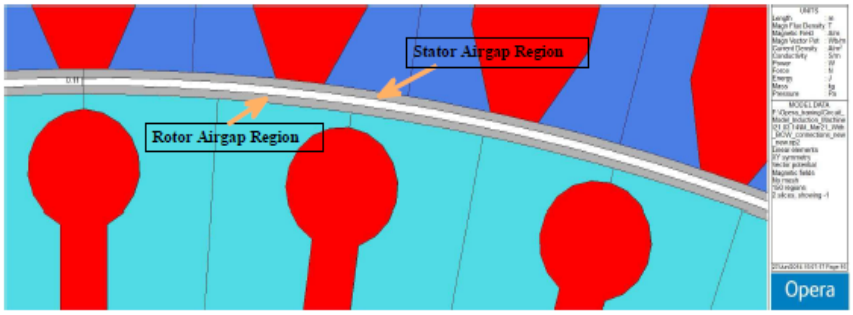


Figure 9. A close view of stator and rotor air gap region

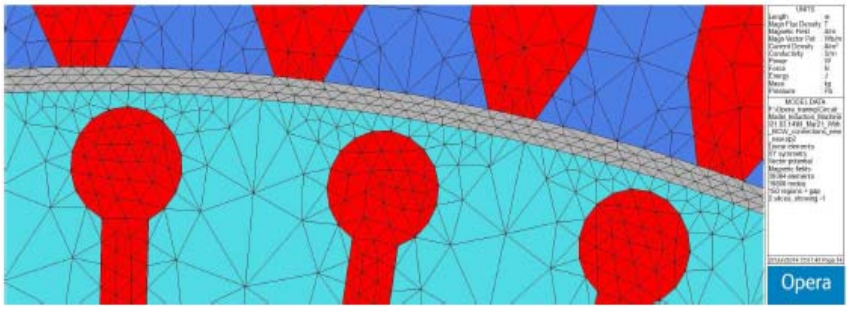


Figure 10. A close mesh view of the stator and rotor air gap region

An external circuit has been coupled with the induction machine model for the transient analysis. Figure 11 shows the external circuit editor in Opera 2D. The GO and the RETURN conductors of the stator winding have been defined in the external circuit editor as shown in Table 2. The external circuit consists of winding coils, resistor, inductor and a functional voltage sources. A *comi* file is a set of functions which has been used to drive the functional voltage sources with the phase difference instead of giving constant amplitude voltage at 50Hz. The rotor bars are short circuited and the effect of rotor skewness is also included in the RM Analysis. Simulations have been done for two different cases of induction machine model. Initially, the induction machine has been modeled without any eccentricity in the Opera 2D model. Later, the machine was modeled with 10% eccentricity of the air gap length. The rotor has been displaced with 10% eccentricity of air gap length ie., ”0.125mm” with the stator. The eccentricity was given in the negative Y-direction in the model. The rotor bars and the rotor core were grouped together as one region in the Opera model and that region was moved to ”-0.125mm” in Y-direction. The FFT of bridge currents and main supply currents have been plotted in MATLABTM by using Opera 2D log results file for both zero eccentricity and 10% eccentricity induction machine models and compared with each other.

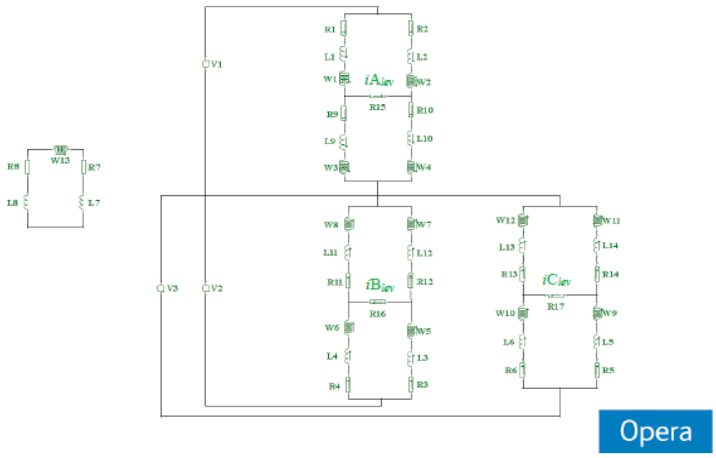


Figure 11. Winding connection in External circuit editor

Table 2. Assigning of Conductor Numbers in the external circuit editor

| Phase Winding | Winding | GO Conductors | Return Conductor |
|---|---|---|---|
| Phase A | W1 | 4, 5, 6, 7, 8 | 79, 80, 81, 82, 83 |
| | W2 | 34, 34, 36, 37, 38 | 109, 110, 111, 112, 113 |
| | W3 | 39, 40, 41, 42, 43 | 114, 115, 116, 117, 118 |
| | W4 | 9, 10, 11, 12, 13 | 84, 85, 86, 87, 88 |
| Phase B | W5 | 54, 55, 56, 57, 58 | 69, 70, 71, 72, 73 |
| | W6 | 24, 25, 26, 27, 28 | 99, 100, 101, 102, 103 |
| | W7 | 29, 30, 31, 32, 33 | 104, 105, 106, 107, 108 |
| | W8 | 59, 60, 1, 2, 3 | 74, 75, 76, 77, 78 |
| Phase C | W9 | 44, 45, 46, 47, 48 | 119, 120, 61, 62, 63 |
| | W10 | 14, 15, 16, 17, 18 | 89, 90, 91, 92, 93 |
| | W11 | 19, 20, 21, 22, 23 | 94, 95, 96, 97, 98 |
| | W12 | 49, 50, 51, 52, 53 | 64, 65, 66, 67, 68 |

## 4. EXPERIMENTAL SETUP

A common 37kW Induction machine is used for the experimental setup shown in Figure 12. The existing stator winding has been removed and replaced by a double layered, distributed, three phase and 4-pole winding. The existing coil wire diameter is ”1.22mm” (18 gauge number). The existing winding is a concentrated winding with 4 strands and 11 turns. It is modified to 3 strands and 11 turns of same wire diameter in order to accommodate the search coil in the main stator slots. Search coils has been used to find the 2-pole. 4-pole and 6-pole field positions. The existing rotor had ”0.8mm” longer shaft. It is modified to ”1.8m” long shaft to make the system flexible. 3300 XL Proximity transducer has been used for the measurement of rotor displacements in three locations shown in Figure 12. In each location, two proximity sensors have been used to measure the rotor responses in X and Y direction. Six voltage transducers have been used to measure the three main phase supply voltages as well as three phase bridge voltages shown in Figure 13. LTS 15- NP (Hall Effect transducer) current transducers were used to measure the three phase bridge currents. The output leads of the proximity sensors, voltage transducer, and current transducers were connected to the Data Acquisition System NI PXI-6221 module through SCB-68 connector box shown in Figure 14. A perforated disc has been inserted in the shaft in order to create the unbalance to the system with the known mass unbalance shown in Figure 15. In the present analysis, only the measured bridge currents have been discussed in order to identify the unbalance present in the system. The output of current transducer is a voltage signal which has a linear correlation with the current.


Figure 12. A modified 37kW Induction machine

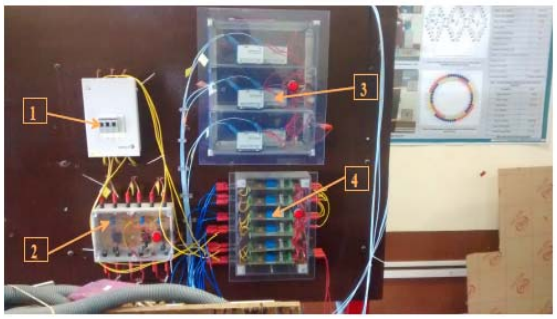

Figure 13. A panel board

In Figure 12, 1 - Bearing Housing at ND end, 2 - Bearing Housing at D end, 3 - Test Machine, 4 – Perforated Disc, 5, 6 and 7 - Locations for the rotor responses, 8- Panel board.

In Figure 13, 1 - Switches for bridges, 2 - Current transducers, 3 - Amplifiers for displacement sensors, 4 - Voltage transducers.

## 5. RESULTS AND DISCUSSION

The important parameters such as main supply current and bridge current have been plotted in MATLAB™ with the use of Opera 2D/RM log file. The comparison of bridge currents and main supply currents of zero eccentricity induction machine model with the 10% static eccentricity induction machine

model has been presented in time domain as well as frequency domain has shown in Figure 16 to Figure 25. Comparison of FFT plots of bridge currents of zero eccentricity model with 10% static eccentricity model has been presented in Figure 26 to Figure 28. Experiments are conducted at 20Hz and 30Hz supply frequency. An amount of 350gm known mass unbalance is introduced in the perforated disc. Bridge currents were measured in two cases ie., when there is no unbalance in the disc and when 350gm known mass unbalance is added to the disc. Experimental results have been presented from Figure 29 to Figure 40.

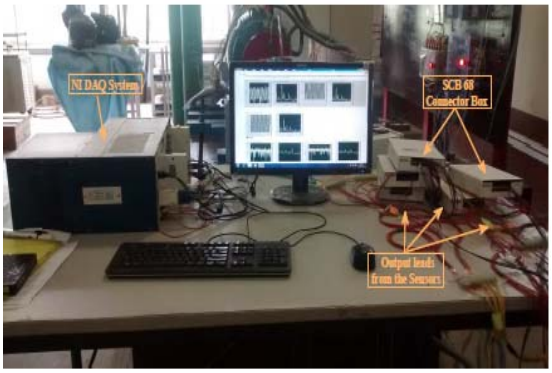


Figure 14. A NI DAQ system

Figure 15. A perforated disc with known mass unbalance

### 5.1. Opera 2D/RM Results for Zero Eccentricity Model

Figure 16 and Figure 17 shows the three phase main supply currents and three phase bridge currents in time domain for zero eccentricity in the model. The FFT of main supply currents and bridge currents have been plotted together in Figure 18 to Figure 20.

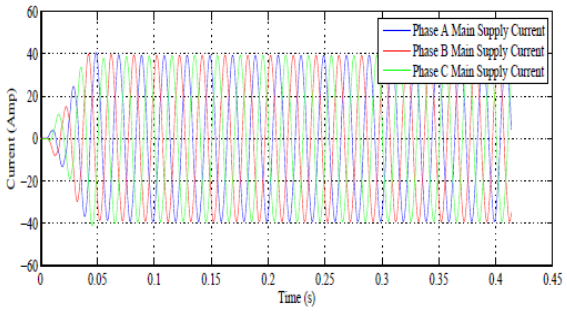


Figure 16. A three phase main supply currents for zero eccentricity model

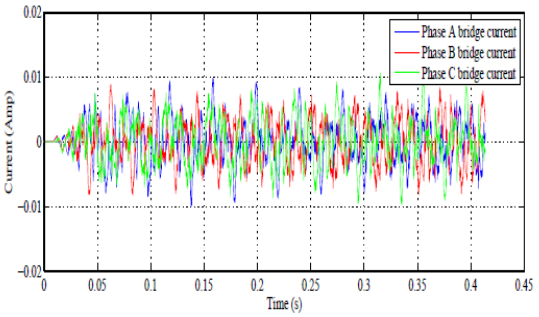


Figure 17. A three phase bridge currents for zero eccentricity model

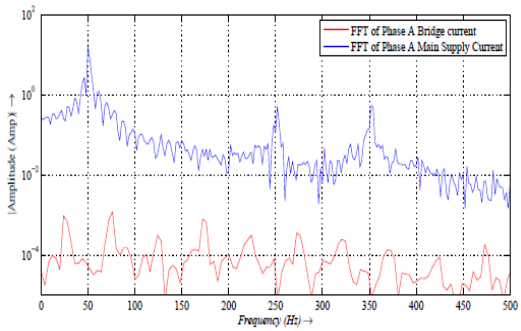


Figure 18. A FFT plot of Phase A bridge current with main supply current at 50Hz for zero eccentricity model

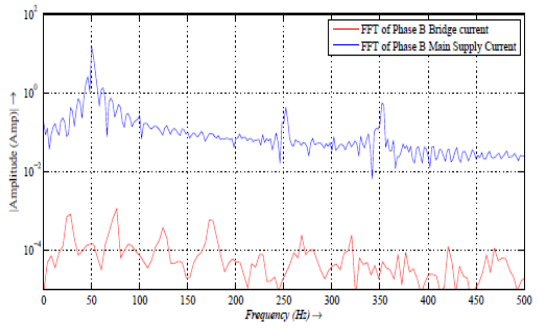


Figure 19. A FFT plot of Phase B bridge current with main supply current at 50Hz for zero eccentricity model

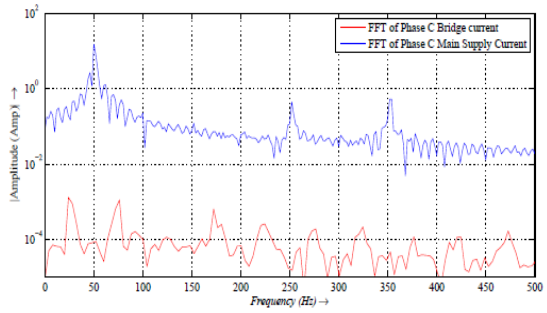


Figure 20. A FFT plot of Phase C bridge current with main supply current at 50Hz for zero eccentricity model

### 5.2. Opera 2D/RM Results for 10% Static Eccentricity Model

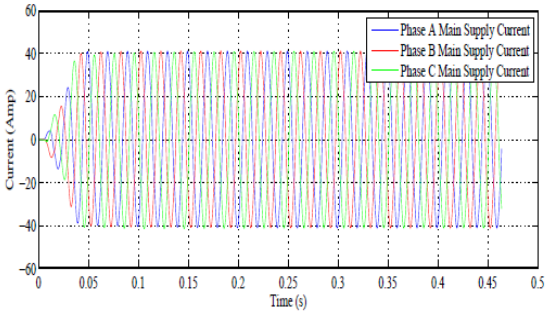


Figure 21. A three phase main supply current for 10% eccentricity model

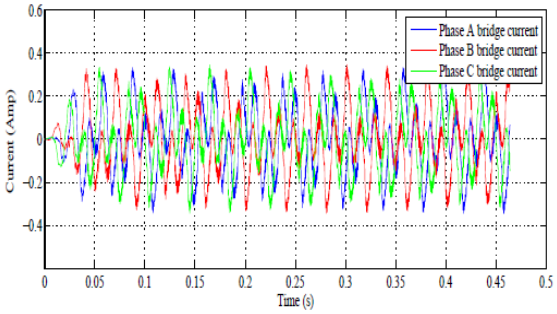


Figure 22. A three phase bridge current for 10% eccentricity model

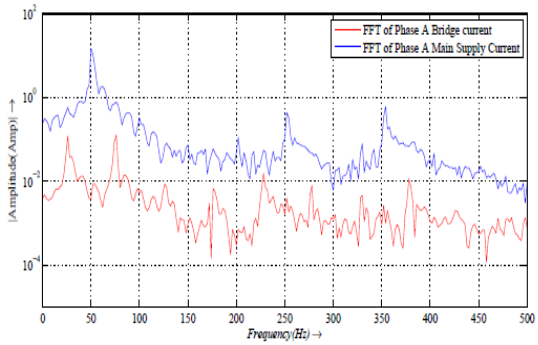


Figure 23. A FFT plot of Phase A bridge current with main supply current at 50Hz for 10% eccentricity model

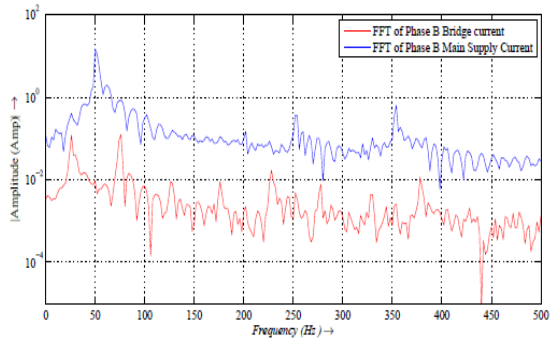


Figure 24. A FFT plot of Phase B bridge current with main supply current at 50Hz for 10% eccentricity model

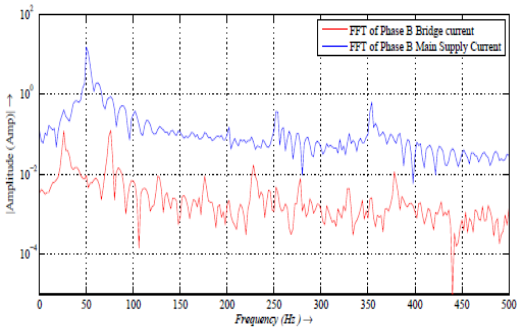


Figure 25. A FFT plot of Phase C bridge current with main supply current at 50Hz for 10% eccentricity mode

Figure 21 and Figure 22 shows the three phase main supply currents and three phase bridge currents in time domain for 10% static eccentricity of the airgap length given in the model. The FFT of main supply currents and bridge currents have been plotted together in Figure 23 to Figure 25.

### 5.3. Comparison of Three Phase Bridge Currents for with and without Eccentricity Model

The bridge currents of zero eccentricity model has been compared with the induced bridge currents of 10% static eccentricity model. Figure 26 to Figure 28 shows the FFT comparison of three phase bridge currents of zero eccentricity model and 10% static eccentricity model.

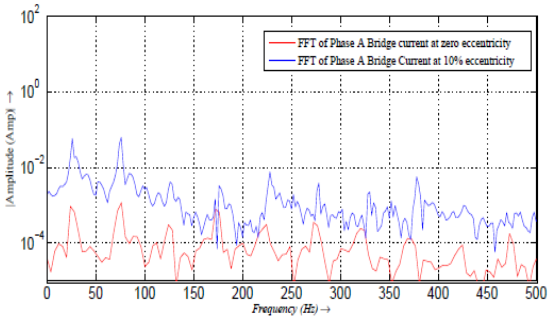


Figure 26. Comparison of FFT plots of Phase A bridge current at zero eccentricity model with 10% eccentricity model

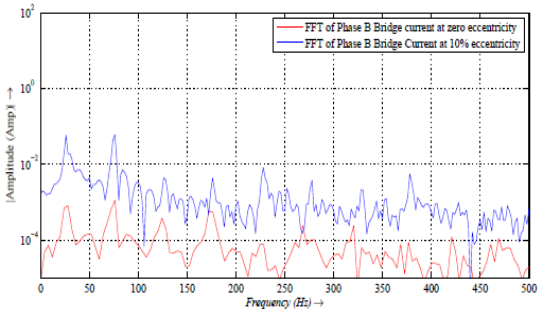


Figure 27. Comparison of FFT plots of Phase B bridge current at zero eccentricity model with 10% eccentricity model

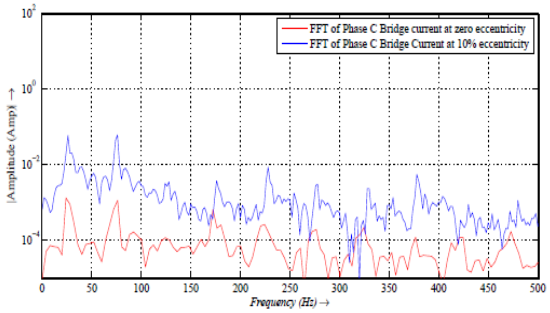


Figure 28. Comparison of FFT plots of Phase C bridge current at zero eccentricity model with 10% eccentricity model

### 5.4. Experimental Results

Experiments have been carried out at 20Hz and 30Hz. The bridge currents have been measured for two cases ie., (i) Without unbalance in the perforated disc, (ii) With 350gm unbalance in the perforated disc. Figure 29 to Figure 34 shows the FFT plots of measured three phase bridge currents when the Bridge is in OFF and ON position. The comparison of FFT plots of measured bridge currents of without unbalance and with the unbalance of 350gm is presented in Figure 35 to Figure 40.

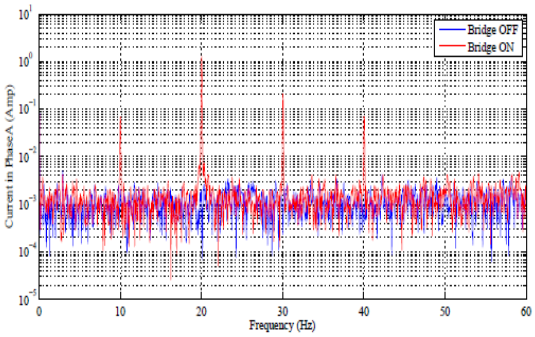


Figure 29. Comparison of Phase A Bridge currents when bridge is in OFF and ON position at 20Hz

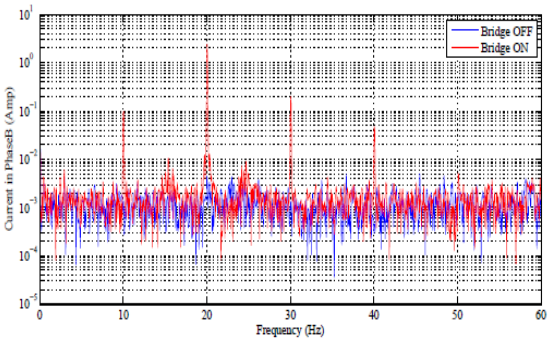


Figure 30. Comparison of Phase B Bridge currents when bridge is in OFF and ON position at 20Hz

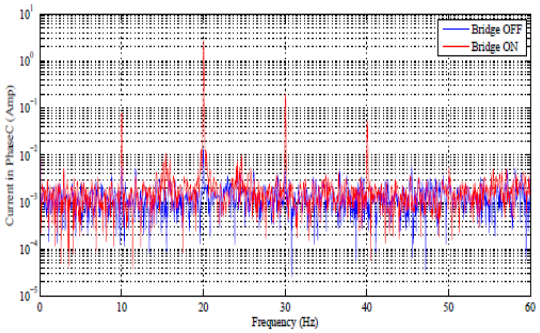


Figure 31. Comparison of Phase C Bridge currents when bridge is in OFF and ON position at 20Hz

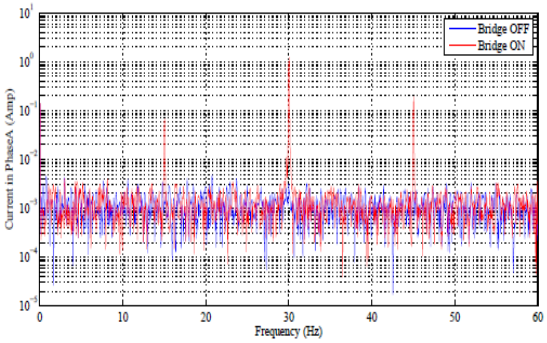


Figure 32. Comparison of Phase A Bridge currents when bridge is in OFF and ON position at 30Hz

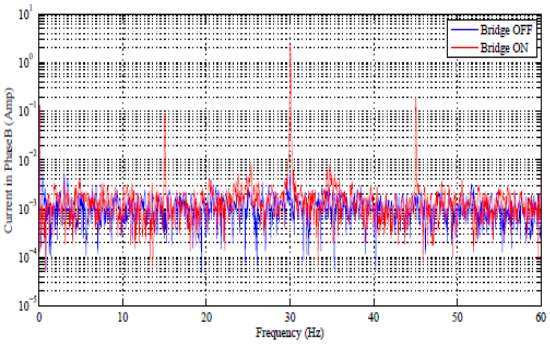


Figure 33. Comparison of Phase B Bridge currents when bridge is in OFF and ON position at 30Hz

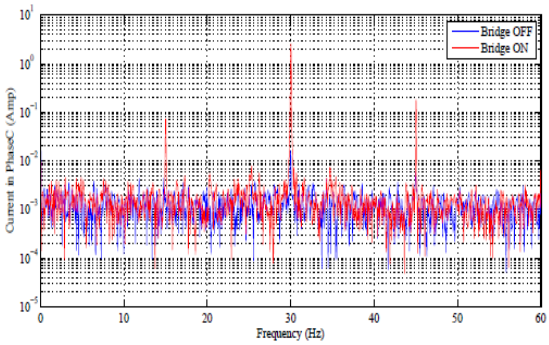


Figure 34. Comparison of Phase C Bridge currents when bridge is in OFF and ON position at 30Hz

### 5.5. Comparison of Three Phase Bridge Currents for with and without Unbalance

Figure 35 to Figure 37 and Figure 38 to Figure 40 shows the FFT plot comparison of bridge currents between no mass in the system and 350gm known mass unbalance in the system at 20Hz and 30 Hz supply frequency respectively.

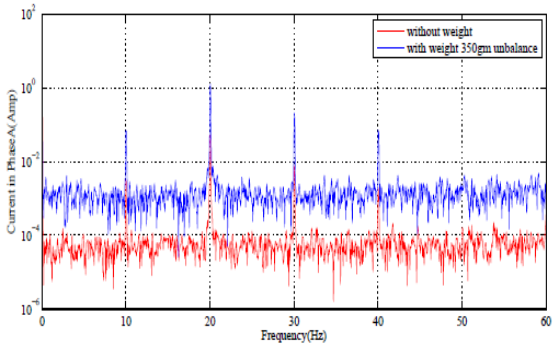


Figure 35. Comparison of Phase A Bridge currents without weight and 350gm unbalance at 20Hz

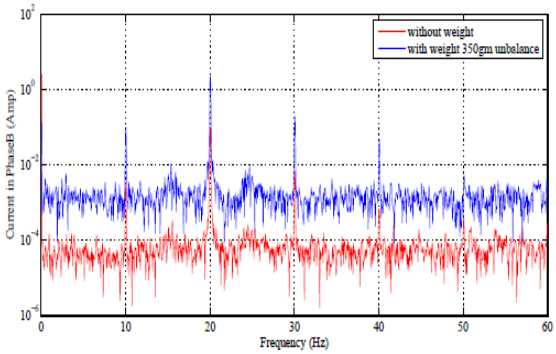


Figure 36. Comparison of Phase B Bridge currents without weight and 350gm unbalance at 20Hz

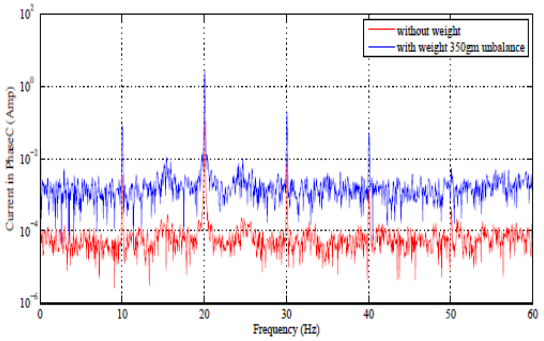


Figure 37. Comparison of Phase C Bridge currents without weight and 350gm unbalance at 20Hz

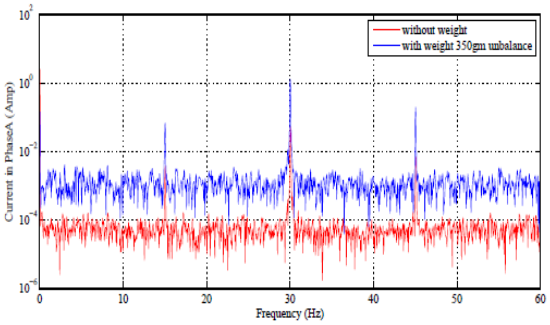


Figure 38. Comparison of Phase A Bridge currents without weight and 350gm unbalance at 30Hz

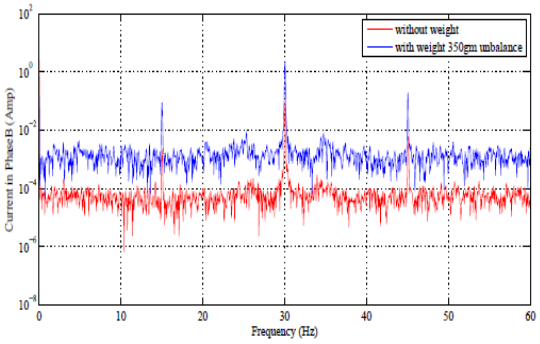


Figure 39. Comparison of Phase B Bridge currents without weight and 350gm unbalance at 30Hz

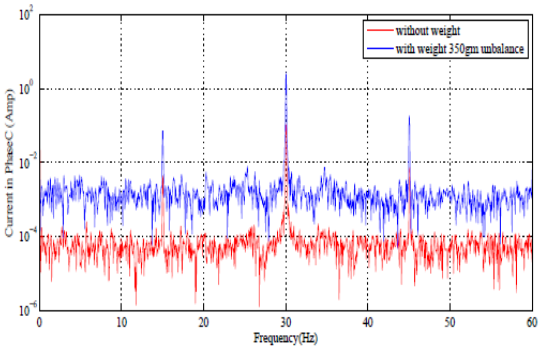


Figure 40. Comparison of Phase C Bridge currents without weight and 350gm unbalance at 30Hz

It has been clearly observed in Opera2D/RM results from Figure 26 to Figure 28 that the bridge currents were flowing in bridges when the eccentricity has been introduced in the model. The dominant frequency components of bridge currents are given by Equation (2) which is presented [13].

$$f_{lev} = f_{sup} \pm f_{rot} \tag{2}$$

Where,

$$f_{rot} = \left\{ (1-s) \times \frac{f_{sup}}{p} \right\}$$

fsup is main supply frequency, s is slip, p is number of pole and frot is rotational frequency.

The comparison of FFT plots for both Opera 2D model shows that the frequency components of bridge currents are 0.51fsup, 1.49fsup where fsup is the main supply frequency. There should be no currents induced in the bridges when the model has zero eccentricity. However, the currents induced in the zero eccentricity model is in the order of ($10^{-2}$ Amps). This may happen due to the modeling error of Opera 2D FE Package. The bridge currents induced in the zero eccentricity model ($10^{-2}$ Amps) are compared with currents induced in the 10% static eccentricity model ($10^{-1}$ Amps). It clearly tells that the bridge currents are flowing when the eccentricity has been introduced in the model. However, 10% static eccentricity of the airgap length is a small amount that may not be high enough to induce more currents in the bridges.

Experimental results show that the bridge current flows in the system even when the perforated disc does not have any known mass unbalance. It clearly indicates that the system has already some unbalance. However, there is no prior knowledge about the unbalance present in the system. It has been observed from Figure 35 to Figure 40 that a comparatively difference in the amplitude of measured currents which are flowing in the bridges when 350gm unbalance is added to the system. It clearly indicates that the flow of bridge currents are increasing with the increase of unbalance in the system.

## 6. CONCLUSION

It has been identified that in all the FFT plots of bridge current has the dominant frequency of 0.51fsup, 1.49fsup where fsup is the main supply frequency. It clearly says that the machine has 2-pole and 6-pole fields due to eccentricity or unbalance present in the system where as 4-pole is the main pole field. Future work has been found that the signature of bridge currents will be analyzed when a tiny amount of three phase AC voltage and DC voltage source will be supplied in the bridges. The main purpose of this present work is to show that the utilization of Opera 2D Finite Element Software in order to incorporate the BCW scheme in the induction machine analysis.

## ACKNOWLEDGEMENT

The authors thankfully acknowledge the financial support from Department of Science and Technology, New Delhi, India.

## REFERENCES

[1] S. Natesan, G. Kumar, K. Kalita, and M. Rahman, "Unbalance detection in flexible rotor using bridge configured winding based induction motor," *Proceedings of the 1st International and 16th National Conference on Machines and Mechanisms (iNaCoMM2013)*, pp. 312–317, 2013.

[2] W. K. S. Khoo, "Ac self-bearing motors with bridge configured winding," Ph.D. dissertation, School of Electrical Engineering, University of Aston, Birmingham, West Midlands, 2002.

[3] W. K. Khoo, "Bridge configured winding for poly-phase self bearing machines," *IEEE Transactions on Magnetics*, Vol. 41, No. 4, pp. 1289–1295, 2005.

[4] A. Laiho, K. Kalita, K. Tammi, and S. D. Garvey, "Dynamics of bridge configured built-in force actuator for vibration control in four-pole cage induction machine," *18th International Congress on Sound and Vibration, ICSV18*, pp. 1–8, 2011.

[5] K. Komeza, M. Dems, and P. Jastrzabek, "The 3d-analysis of the field distribution of fractional power induction motor," *11th International Symposiyum on Electromagnetic Fields in Electrical Engineering,ISEF11*, pp. 137–142, 2008.

[6] C. Riley, A. Michaelides, K. Hoffer, D. Griffiths, and J. Sykulski, "Automation of finite element aided design of induction motors using multislice 2d model," *The International Journal for Computation and Mathematics in Electrical and Electronics Engineering*, Vol. 25, No. 2, pp. 309–319, 2009.

[7] K. Komeza, M. Dems, and P. Jastrzabeki, "Experimental verification of field-circiut finite elements models of induction motors feed from inverter," *Recent Developments of Electrical Drives*, Springer, pp. 275–289, 2009.

[8] M. N. Syatirah, N. H. Halim, I. Daut, Y. Yanawati, N. Shafiqin, N. Gomesh, and M. Asri, "Design and mideling of 1-phase induction motor using opera 2d software based on copper material," *PEOCO2011, IEEEXPLORE*, pp. 193–196, 2011.

[9] Y. Yanawati, I. Daut, S. N. Shafiqin, I. Pungut, M. N. Syatirah, N. Gomesh, A. R. S. Rafidah, and N. Haidar, "Efficiency increment on 0.35 mm and 0.50 mm thichness of non-oriented steel sheets for 0.5 hp induction motor," *International Journal of Materials Engineering*, Vol. 2, No. 2, pp. 1–5, 2012.

[10] I. Daut, N. Gomesh, Y. Yanawati, M. Irwanto, S. N. Shafiqin, and Y. Irwan, "Modeling and simulation of 0.5 hp rotating machine for the investigation of losses by using copper as rotor bar material," *Australian Journal of Basic and Applied Sciences*, Vol. 5, No. 12, pp. 170–188, 2011.

[11] A. M. Michaelides, C. P. Riley, and S. Taylor, "Dynamic analysis of linear and rotary electrical machines," *IEEE Transaction*, 2011.

[12] J. Kappatou, K. Gyftakis, and A. Safacas, "Fem study of the rotor slot design influences on the induction machine characteristics," *Advanced Computer Techniques in Applied Electromagnetics*, IOS Press, Vol. 30, pp. 247–252, 2008.

[13] R. S. Konwar, K. Kalita, A. Banerjee, and W. K. S. Khoo, "Electromagnetic analysis of a bridge configured winding cage induction machine using finite element method," *Progress in Electromagnetics Research B*, Vol. 48, No. 4, pp. 347–373, 2013.